Electrostatic Potential Fluctuations Near Electrode Interfaces

Aditya M. Limaye*
Department of Chemical Engineering, MIT, Cambridge, MA 02139
(Dated: May 17, 2019)

Fluctuations of the electrostatic potential near an electrode interface play an important role in interfacial electron transfer processes. Molecular dynamics simulations suggest that the magnitude of fluctuations in the electrostatic potential is strongly suppressed near an electrode interface compared to the bulk electrolyte. In this paper, we use continuum electrostatics to develop a simple statistical field theory that captures the origin of this fluctuation attenuation near a constant-potential interface. We compare predictions from this theory to results from atomistic molecular simulations. We conclude by discussing possible improvements to the theory, and its implications for understanding electrochemical systems.

I. INTRODUCTION

A number of emerging and established energy technologies (fuel cells, batteries, etc.) rely on driving electron transfer (ET) reactions between metal interfaces and redox-active chemical species in the solution phase. Marcus, in work that received the 1992 Nobel Prize in Chemistry, developed the first quantitative kinetic theory of ET reactions in bulk solution. The success of Marcus theory is due to its serious treatment of environmental solvation effects, which exert a controlling effect on the kinetics of ET in condensed phases.

Marcus theory posits that ET events are concomitant with rare solvent reorganization events which render the initial and final states of a redox reaction isoenergetic [1]. Interactions between solvent molecules and redox-active species are primarily electrostatic, so these reorganization events result in atypical values of the environmentally-exerted electrostatic potential on a redox-active species. Marcus derived his famous rate equation by assuming that the electrostatic potential distributions on an ionic species are Gaussian around their mean [2]. The variance of these Gaussian distributions comprises the only free parameter in Marcus theory, often termed the "reorganization energy".

Planar interfaces between an electrode and electrolyte break the translational symmetry of the liquid phase, resulting in many interesting anisotropies [3, 4]. Molecular dynamics simulations have demonstrated (see Appendix A) that the variance of electrostatic potential distributions decreases sharply upon approaching an electrode interface held at constant potential. This result is surprising, because the distribution of ionic charge density is *not* anisotropic; it has position-independent variance.

Here, we develop a simple statistical field theory that quantitatively captures the suppression of electrostatic potential fluctuations near constant potential interfaces. We include interactions to linear order under the framework of Debye-Hückel theory, and compare with results from molecular simulations. We conclude by speculating about the effects of departures from Debye-Hückel screening behavior, as would be present in a concentrated electrolyte solution.

II. PRELIMINARIES

An electrochemical cell is comprised of an electrolyte solution "sandwiched" between two metal electrodes, between which a constant potential difference can be maintained. By linearity, the potential profile in the cell can be split into a fluctuating component which is fixed at zero at the cell boundaries, and a deterministic component imposing the constant potential difference. Since our primary concern is characterizing fluctuations in the potential, we need only consider the former component of the potential.

Although a realistic cell is three-dimensional, for the purposes of this paper, we will slab-average quantities over coordinates orthogonal to the electrode approach coordinate, resulting in a one-dimensional field theory. Figure 1 presents a schematic description of electrochemical cell domain.

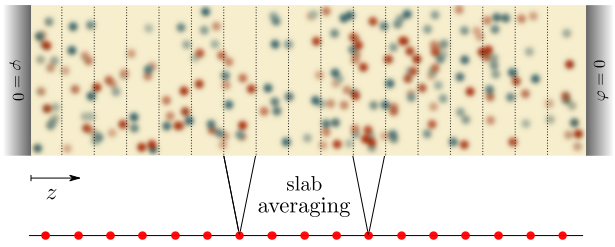

FIG. 1. Schematic of electrochemical cell domain.

Without loss of generality, we can scale the electrode approach coordinate $z \in [0, 1]$. We are interested in two fluctuating fields inside this domain, the ionic charge density $\rho(z)$ and the electrostatic potential $\varphi(z)$ that the charge density induces. Under the framework of continuum electrostatics, these two fields are related by Poisson's equation:

$$\varphi_{zz} = -4\pi\rho \tag{1}$$

* amlimaye@mit.edu

Eq. (1) is an elliptic PDE, so we need to specify the value of φ at all boundary points. Based on our constant potential constraint, we impose $\varphi(0) = \varphi(1) = 0$.

One clever way to satisfy the constant potential boundary conditions is to employ the method of images. This requires considering a mirrored array of equal but opposite charges to the distribution $\rho(z)$ lying in the mirror domain $[-1, 0]$. Including this extra array of charges automatically enforces $\varphi(0) = 0$. From here on, we will assume that $\rho(z)$ is a function supported on the interval $[-1, 1]$ which is required to be odd to satisfy the mirror symmetry. We still have to satisfy the $\varphi(1) = 0$ boundary condition. This can be done with an appropriate choice of basis functions.

The Fourier sine series with integer frequencies comprises a complete basis for odd functions f that also satisfy the constraint $f(1) = 0$. These basis functions have the form:

$$\psi_q(z) = \sin(qz) \tag{2}$$

where we define $q \equiv n\pi$, with $n \in \mathbb{Z}^+$. Define an inner product as follows:

$$\langle f|g\rangle = \int_{-1}^{1} dz f(z)g(z) \tag{3}$$

It is easy to see that the sinusoidal basis functions are orthogonal, $\langle \psi_k|\psi_q\rangle = \delta_{kq}$. The Fourier sine transform $\hat{f}(q)$ of a function $f(z)$ is defined by:

$$f(z) = \sum_{q=0}^{\infty} \hat{f}(q)\psi_q(z) \tag{4}$$

In this basis, standard transformations of Poisson's equation yield:

$$q^2\hat{\varphi}(q) = 4\pi\hat{\rho}(q) \tag{5}$$

In any electrolyte solution with mobile charges, Poisson's equation provides an snapshot of the electrostatic potential given an instantaneous charge density, but is inappropriate for describing the *average* potential, because it neglects correlations between mobile charges. The nonlinear Poisson-Boltzmann equation fully accounts for such correlations, but is unamenable to pen-and-paper analysis. Debye-Hückel theory is a linearization of the Poisson-Boltzmann equation that incorporates screening effects to linear order. Formally,

$$\varphi_{zz} - 4\pi\kappa^2\varphi = -4\pi\rho \tag{6}$$

The parameter $\kappa = \lambda^{-1}$, where λ is the Debye screening length, which goes inversely with the ionic strength of the solution. Again with standard transformations, we can arrive at:

$$\left(q^2 + 4\pi\kappa^2\right)\hat{\varphi}(q) = 4\pi\hat{\rho}(q) \tag{7}$$

III. MODEL

Simulation data indicates that the fluctuating charge density has position-independent variance. The simplest possible model we can write for this fluctuating field is a pointwise Gaussian theory with a single free variance parameter,

$$\mathcal{P}\left[\rho(z); \sigma_\rho\right] \propto \exp\left[-\left(2\sigma_\rho^2\right)^{-1} \int_{-1}^{1} dz \rho(z)^2\right]. \tag{8}$$

Passing to Fourier space yields, as usual, an uncorrelated distribution that factorizes over the Fourier sine modes,

$$\mathcal{P}\left[\hat{\rho}(q); \sigma_\rho\right] \propto \prod_q \exp\left[-\frac{\hat{\rho}(q)^2}{2\sigma_\rho^2}\right]. \tag{9}$$

In plain terms, every frequency component of the charge density is drawn independently from a Gaussian of equal variance (they are iid).

A. Unscreened Potentials

The induced distribution over the electrostatic potential is independent, but not identically distributed over the Fourier sine modes. Applying Eq. (5),

$$\mathcal{P}\left[\hat{\varphi}(q); \sigma_\rho\right] \propto \prod_q \exp\left[-\frac{q^4}{32\pi^2\sigma_\rho^2} \cdot \hat{\varphi}(q)^2\right] \tag{10}$$

Hence, the frequency components of the induced potential are drawn independently from Gaussians with variance that decreases as the frequency to the fourth power.

We can reconstruct the real space potential via inverse Fourier transform. The Fourier components of the potential are random variables (RVs) drawn from normal distributions with different variances. Using $\mathcal{N}(\mu, \sigma^2)$ to denote a normal RV with mean μ and variance σ^2, we have

$$\varphi(z) = \sum_q \mathcal{N}\left(0, \frac{16\pi^2\sigma_\rho^2}{q^4}\right) \sin(qz) \tag{11}$$

Employing standard Gaussian scaling rules and exploiting the fact that variances of independent RVs simply sum,

$$\mathrm{Var}\left[\varphi(z)\right] = \frac{16\sigma_\rho^2}{\pi^2} \sum_{n=1}^{\infty} \frac{\sin^2(n\pi z)}{n^4} \tag{12}$$

An analytical result for this summation is known (Eq. (B4)). Figure 2 depicts a plot of the analytical variance profile, as well as a result from straightforward numerical sampling of the distribution in Eq. (10).

Indeed, this simple theory reproduces the position-dependent variance observed in molecular dynamics simulations. This phenomenon is a straightforward consequence of the fact that the potential must be smoother

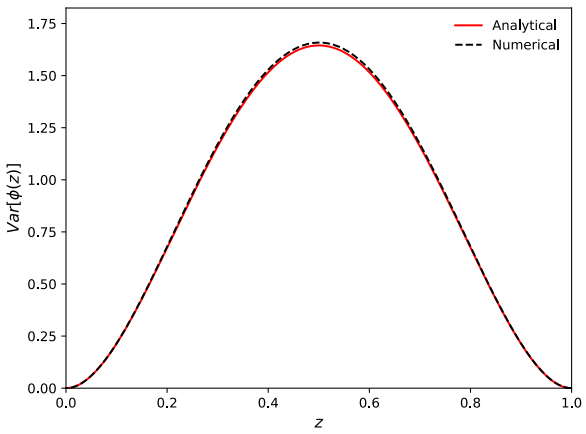

FIG. 2. A plot of the closed-form analytical result for Eq. (12) compared with results from numerical sampling of the distribution in Eq. (10). In both cases, $\sigma_\rho^2 = 1$.

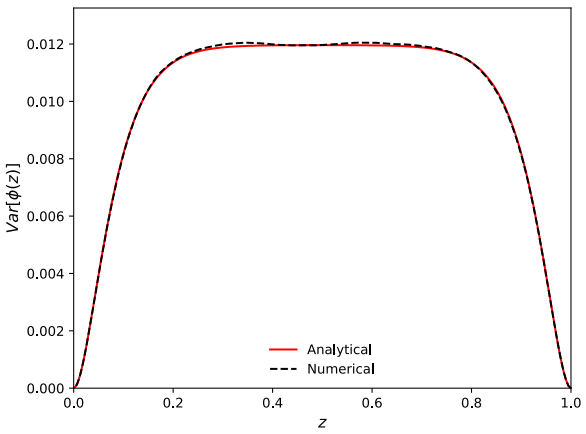

FIG. 3. A plot of the closed-form analytical result for Eq. (14) compared with results from numerical sampling of the distribution in Eq. (13). In both cases, $\sigma_\rho = 1$ and $\lambda = 0.30$.

than the charge density that generates it. Near the boundary at $z = 0$, all Fourier sine modes are increasing roughly linearly. As indicated by Eq. (10), the high frequency modes, which increase fastest near $z = 0$, are attenuated by a factor of q^4, resulting in suppression of the variance in electrostatic potential near the boundary.

B. Screened Potentials

Despite this success, the variance profiles depicted in Fig. 2 disagree with simulation results for large cells. Once the cell length z_{cell} becomes large compared to the Debye screening length λ, the variance profile must plateau for $z > \lambda$, since the electrostatic influence of the electrode is effectively screened.

In order to incorporate a screening length scale, we must modify the induced distribution over the electrostatic potential in accordance with Debye-Hückel theory. Applying Eq. (7),

$$\mathcal{P}\left[\hat{\varphi}(q)\right] \propto \prod_q \exp\left[-\frac{\left(q^2 + 4\pi\kappa^2\right)^2}{32\pi^2\sigma_\rho^2} \cdot \hat{\varphi}(q)^2\right] \tag{13}$$

Following an analogous Fourier inversion procedure,

$$\text{Var}\left[\varphi(z)\right] = \frac{16\sigma_\rho^2}{\pi^2} \sum_{n=1}^{\infty} \frac{\sin^2(n\pi z)}{\left(n^2 + 4\kappa^2/\pi\right)^2} \tag{14}$$

An analytical result for this summation is known (Eq. (B5)). Figure 3 depicts a plot of the analytical variance profile, as well as a result from straightforward numerical sampling of the distribution in Eq. (13).

Introducing the Debye screening length scale λ reproduces the expected behavior; for $z > \lambda$, the variance profile plateaus, since the influence of the electrode is entirely attenuated by ionic screening. Additionally, for identical values of σ_ρ, the maximum magnitude of the variance is cut by two orders of magnitude compared to the unscreened case.

IV. DISCUSSION

In this paper, we have developed a statistical field theory that explains the suppression of fluctuations in the electrostatic potential near an electrode interfaces, a phenomenon observed in molecular simulations. Simple Fourier analysis reveals that the the fluctuation attenuation is a direct consequence of the requirement that the potential be smoother than its charge density, as well as the constant potential boundary condition. Our model includes correlations between ions to linear order under the framework of Debye-Hückel theory, which act to screen away the influence of the electrode beyond the electrostatic screening length λ.

Additional interesting behavior may emerge if stronger ionic correlations are treated properly. Debye-Hückel theory is only valid at low ion concentrations, and phenomena such as ion overscreening and crowding, characterized in the context of ionic liquids [5], may serve to extend the influence of the electrode, creating long-range ionic correlations.

In the context of ET kinetics and Marcus theory, the results presented here suggest that the solvent environment becomes harder to re-organize upon approaching an electrode. Naively, this would suggest a suppression of ET rates near an interface compared to the bulk, an effect that may be observable with careful experiments that deconvolute other interfacial effects (changing ionic activities, double-layer effects, etc.).

ACKNOWLEDGMENTS

The author wishes to acknowledge Prof. Mehran Kardar for teaching a course in statistical mechanics that was nothing short of excellent. The author would also like to express gratitude towards Prof. Adam Willard and Dr. Wendu Ding for useful discussions related to this work.

Appendix A: Results from Molecular Simulations

We performed molecular simulations on a system of positive and negative ions between two metal electrodes held at constant potential using standard methods. Solvent was treated implicitly by imposing an effective dielectric constant attenuating all electrostatic interactions. Figure 4 shows a snapshot of the simulation geometry.

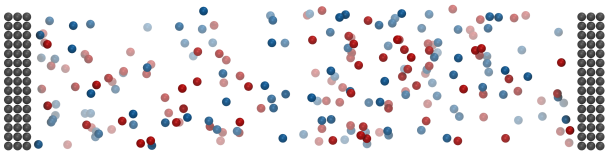

FIG. 4. Geometry of a simulation cell. Gray atoms correspond to metal electrode atoms, which are held at constant potential $\varphi = 0$. Blue (red) spheres are negative (positive) ions, both carrying unit charge.

Two important results emerge from analysis of data generated from molecular simulations. First the distribution of the ionic charge density has roughly constant variance across the length of the simulation cell. The ionic charge density can be determined at each point in the simulation cell using a fairly standard Gaussian charge spreading scheme. Figure 5 depicts traces of the effective free energy for the ionic charge density, gleaned from simulation statistics. Each curve looks parabolic, a indicating a Gaussian distribution. Most importantly, the curvature of the parabolas is roughly constant across different z-traces, indicating a position-independent variance.

For each simulation snapshot, we can compute a Poisson potential at each point in the simulation cell using Eq. (1). Figure 6 depicts traces of the effective free energy for the potential at various values of z. The behavior of these curves is qualitatively different than those shown in Fig. 5. The parabola curvature increases sharply as $z \to 0$, indicating an electrostatic potential variance that decreases sharply upon approaching the electrode.

Appendix B: Analytical Expressions for Summations

The analytical results for the summations encountered when performing Fourier inversion are reported here. They are expressed in terms of certain special functions,

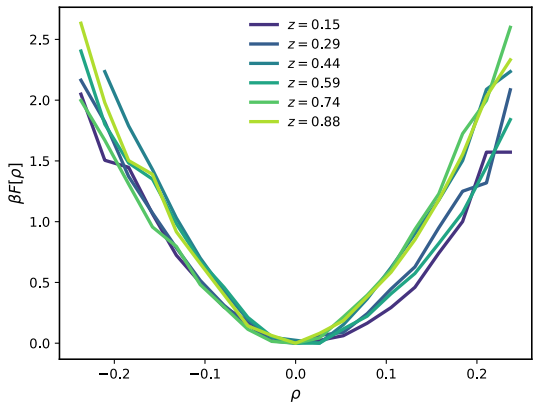

FIG. 5. Effective free energy $\beta F[\rho(z)]$ for the ionic charge density field, computed from simulation statistics.

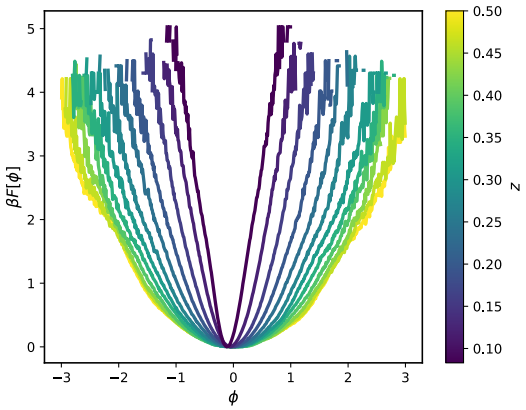

FIG. 6. Effective free energy $\beta F[\varphi(z)]$ for the potential field, computed from simulation statistics.

which we will define before showing the analytical results. First, the Hurwitz-Lerch transcendent:

$$\Phi_{\mathrm{HL}}(z, s, \alpha) \equiv \sum_{n=0}^{\infty} \frac{z^n}{(n+\alpha)^s} \tag{B1}$$

Second, the Gamma function:

$$\Gamma(z) \equiv \int_0^{\infty} x^{z-1} e^{-x} dx \tag{B2}$$

Finally, the Gauss hypergeometric function:

$${}_2F_1(a, b; c; z) \equiv \frac{\Gamma(c)}{\Gamma(b)\Gamma(c-b)} \cdot \int_0^1 \frac{t^{b-1}(1-t)^{c-b-1}}{(1-tz)^a} dt \tag{B3}$$

The results for the unscreened and screened case, respectively, are

$$\mathrm{Var}\left[\varphi(z)\right] = \frac{4\sigma_\rho^2}{45\pi^2}\left[\pi^4 - 45\left\{e^{i2\pi nz}\Phi_{\mathrm{HL}}(e^{i2\pi nz},4,1) + e^{-i2\pi nz}\Phi_{\mathrm{HL}}(e^{-i2\pi nz},4,1)\right\}\right] \tag{B4}$$

$$\begin{aligned}\mathrm{Var}\left[\varphi(z)\right] = \frac{\sigma_\rho^2}{4\kappa^4}\Bigg\{ & -1 + \sqrt{\pi}\kappa\cdot\coth\left(2\sqrt{\pi}\kappa\right) + 2\pi\kappa^2\cdot\mathrm{csch}^2\left(2\sqrt{\pi}\kappa\right)^2 \\ & + \pi^{-1}e^{-2\pi iz}\kappa^2\cdot\Bigg[\Phi_{\mathrm{HL}}\left(e^{2\pi iz},2,1-\frac{2i\kappa}{\sqrt{\pi}}\right) + \Phi_{\mathrm{HL}}\left(e^{-2\pi iz},2,1+\frac{2i\kappa}{\sqrt{\pi}}\right) \\ & \quad + \Gamma\left(-\frac{2i\kappa}{\sqrt{\pi}}\right){}_2F_1\left(1,1-\frac{2i\kappa}{\sqrt{\pi}};2-\frac{2i\kappa}{\sqrt{\pi}};e^{-2\pi iz}\right) \\ & \quad + \Gamma\left(+\frac{2i\kappa}{\sqrt{\pi}}\right){}_2F_1\left(1,1+\frac{2i\kappa}{\sqrt{\pi}};2+\frac{2i\kappa}{\sqrt{\pi}};e^{-2\pi iz}\right)\Bigg] \\ & + \pi^{-1}e^{+2\pi iz}\kappa^2\cdot\Bigg[\Phi_{\mathrm{HL}}\left(e^{2\pi iz},2,1-\frac{2i\kappa}{\sqrt{\pi}}\right) + \Phi_{\mathrm{HL}}\left(e^{-2\pi iz},2,1+\frac{2i\kappa}{\sqrt{\pi}}\right) \\ & \quad + \Gamma\left(-\frac{2i\kappa}{\sqrt{\pi}}\right){}_2F_1\left(1,1-\frac{2i\kappa}{\sqrt{\pi}};2-\frac{2i\kappa}{\sqrt{\pi}};e^{-2\pi iz}\right) \\ & \quad + \Gamma\left(+\frac{2i\kappa}{\sqrt{\pi}}\right){}_2F_1\left(1,1+\frac{2i\kappa}{\sqrt{\pi}};2+\frac{2i\kappa}{\sqrt{\pi}};e^{-2\pi iz}\right)\Bigg]\Bigg\}\end{aligned} \tag{B5}$$

Appendix C: Analysis of Screened Potential Result

The analytical result for the variance profile of the screened electrostatic potential in Eq. (B5) is rather opaque. The original summation in Eq. (14) (reproduced below) presents some opportunities for analysis to extract its qualitative behavior.

$$\mathrm{Var}\left[\varphi(z)\right] = \frac{16\sigma_\rho^2}{\pi^2}\sum_{n=1}^{\infty}\frac{\sin^2(n\pi z)}{\left(n^2+4\kappa^2/\pi\right)^2} \tag{C1}$$

Symmetry of the problem demands that the function is symmetric around $z = 0.5$. It is also apparent that $\mathrm{Var}[\varphi(0)] = 0$, since $\sin(0) = 0$.

Less apparently, this function must plateau for values of $\kappa z > 1$. To see why, first note that the sum is well-approximated by only considering frequencies up to a cutoff κ, since higher frequency components are killed quickly by a factor of q^4. These "relevant" frequency components can all be linearized to good approximation by qz for $\kappa z \ll 1$. In this range, all of these frequency components are increasing, and so $\mathrm{Var}[\varphi(z)]$ is also increasing. The linearization fails after $\kappa z \approx 1$, since the highest relevant frequency component begins to plateau and then decrease. For $z \gg \kappa^{-1}$, the sum runs over nearly orthogonal functions, and hence does not change much with z.

[1] D. Chandler, Electron transfer in water and other polar environments, how it happens, in *Classical and Quantum Dynamics in Condensed Phase Simulations* (WORLD SCIENTIFIC, 2010) pp. 25–49.

[2] R. A. Marcus, On the Theory of OxidationReduction Reactions Involving Electron Transfer. I, The Journal of Chemical Physics **24**, 966 (1956).

[3] S. Shinand A. P. Willard, Three-Body Hydrogen Bond Defects Contribute Significantly to the Dielectric Properties of the Liquid Water-Vapor Interface, Journal of Physical Chemistry Letters **9**, 1649 (2018).

[4] J. A. Kattirtzi, D. T. Limmer, and A. P. Willard, Microscopic dynamics of charge separation at the aqueous electrochemical interface **114**, 10.1073/pnas.1700093114 (2017), arXiv:1703.02216.

[5] M. Z. Bazant, B. D. Storey, and A. A. Kornyshev, Double layer in ionic liquids: Overscreening versus crowding, Physical Review Letters **106**, 6 (2011).